Tellus (1990), *42A*, 174–193

The role of synoptic/planetary-scale interactions during the development of a blocking anticyclone

By CHIH-HUA TSOU and PHILLIP J. SMITH, *Department of Earth and Atmospheric Sciences, Purdue University, West Lafayette, Indiana 47907, USA*

(Manuscript received 5 September 1988; in final form 20 December 1988)

ABSTRACT

The period 19–21 January 1979 marked the development of a blocking anticyclone over the North Atlantic Ocean preceded by explosive cyclogenesis about 500 km south of Nova Scotia. Using fields derived from GLA analyses (4° lat × 5° long) of the FGGE SOP-I data set, the general behavior of this block is diagnosed using the extended height tendency equation. This equation preserves much of the simplicity of the quasi-geostrophic form, but replaces the geostrophic wind and relative vorticity by the observed value. Three-dimensionally varying static stability and strong diabatic heating are also allowed in the extended form. To further analyze the relative importance of planetary-scale, synoptic-scale, and scale-interaction forcing of this block, height tendencies were solved from a scale-partitioned form of height tendency equation. The scale partitioning is accomplished using the Barnes objective analysis scheme. Results indicate that vorticity advection was the primary forcing mechanism during the block development. Growth in this mechanism occurred during and extended beyond the period of explosive cyclogenesis and was located downstream from the cyclone event. In fact, much of the vorticity advection was attributed to the northward advection of negative relative vorticity east of a jet streak that formed between the cyclone and anticyclone. The scale interactions implied by this relationship between the cyclone and anticyclone were confirmed in the partitioned height tendencies. The scale-interaction component was consistently larger than the other two and was particularly significant during the block development. This component was followed in importance by the synoptic-scale component, although the latter was significant only in the vorticity advection term. Interestingly, despite pronounced northward warm air advection, the direct forcing of the block by thermal advection was relatively small. Rather, the thermal forcing was strongest in the upstream cyclone, which in view of the subsequent role of scale interactions in the block development suggests an indirect role for thermal advection.

1. Introduction

Large-scale circulation anomalies have received considerable attention in recent years. Particularly significant have been those associated with blocking anticyclones, defined in synoptic terms as warm, large-scale stationary ridges or anticyclones that form over high latitudes and persist for several days. According to Rex (1950), there are two preferred locations for blocking occurrence, one over the eastern Pacific Ocean (Pacific blocking) and the other over the eastern Atlantic Ocean (Atlantic blocking). These two blocking patterns may exist simultaneously. However, Rex (1950) found that such double blocks are normally short lived and single blocks are more frequently found in the general circulation pattern. Lejenäs and Økland (1983) showed that occurrences of these two type of blockings are independent of each other. This implies that most blocking cases are basically local phenomena.

The physical processes responsible for the evolution of blocking are still under investigation. Using a barotropic flow model, Thompson (1957) showed that a sharp jet in middle latitudes can split into two jet streams in the pure barotropic flow. Based on this study Thompson concluded that the initiation and development of blocking is essentially a barotropic process. However, Egger (1978) pointed out that blocking is not entirely a barotropic phenomenon. In fact, White and Clark (1975) suggested that baroclinic instability modified by sensible heat exchange is responsible for the development of blocking over the central North Pacific, since the formation of blocking ridges occurs most often in autumn and winter months when the mid-latitude westerlies and sensible heat exchange between ocean and atmosphere are at their maximum values. Using a two-layer spherical quasi-geostrophic model to study the instability properties of three-dimensional Northern Hemisphere average winter flow, Frederiksen (1983) suggested that the development of mature anomalies such as blocks may be thought of as essentially a two-stage process. During the stage of rapid growth and eastward propagation, the disturbance grows through the combined baroclinic-barotropic instability of the three-dimensional basic state. As the disturbance increases its zonal scale and becomes stationary, the unstable mode amplifies without phase propagation and equivalent barotropic effects become dominant.

Charney and DeVore (1979) and Charney et al. (1981) proposed that blocking is a manifestation of multiple equilibrium states and, further, that these states can be externally forced (e.g., by orography, surface thermal contrast, etc.). Using a highly truncated barotropic spectral model they found that in some parameter regions there are two stable (high-index and low-index circulation) and one unstable equilibrium states. The block is an example of low index circulation. The transition from low-index to high-index state occurs via the instability of the unstable state. Charney and Straus (1980) also found multiple equilibrium states using a two-layer baroclinic model. Observational confirmation has been provided by Sutera (1986), who found that the probability density distribution of the amplitude of the planetary-scale wave formed by zonal harmonic wavenumbers 2–4 is bimodal. Examining stationary wave structures and mean spectral energy and enstrophy budgets, Hansen (1986) further confirmed the existence of the planetary-wave bimodality. Hansen also noted that the stationary large-scale wave of high amplitude appears more hemispheric in character and is primarily maintained by stationary baroclinic forcing. However, the Rex-type blocking events characterized by more regional synoptic patterns are dominated by the non-linear interactions between cyclone and large-scale waves. Tung and Rosenthal (1985) and Cehelsky and Tung (1987) re-examined the multiple equilibrium in a fully non-linear barotropic and baroclinic model, respectively. They found only one weather regime for the large-scale flow. They hypothesize that in the barotropic model of Charney et al. (1981) the importance of non-linear interactions between waves and the mean shear is truncated, while in the baroclinic model of Charney and Straus (1980) the only non-linear interaction represented is the interaction between waves and mean flow.

Recently, intense upstream wave-cyclones have received increasing attention as a possible forcing mechanism since such phenomena are often found to precede the growth of a downstream blocking ridge. The heat and momentum transfer by these traveling cyclones may have important impacts on the evolution of blocking ridges, although the typical blocking flow patterns are of larger scale. Green (1977) postulated that the block linked to the British drought of 1976 could have been maintained by the transfer of momentum by synoptic-scale eddies. Hansen and Chen (1982) performed a case study of a block in the Atlantic Ocean and found that the non-linear transfer of energy from intense baroclinic cyclone waves to the barotropic ultralong waves provided the major source of kinetic energy of the block. Austin's (1980) and Shutts's (1983) modeling results indicated that anticyclonic eddy forcing tended to be one-quarter wavelength upstream of the blocking wave and opposed the tendency for the blocks to be advected downstream by the time mean flow. Observational evidence provided by Illari (1984) and Mullen (1987) further support the quadrature relationship between the synoptic-scale forcing and the blocking episode. Mullen (1987) suggested that this quadrature relationship is primarily due to vorticity transports associated with synoptic-scale disturbances. Comparing blocking versus non-blocking planetary-scale circulation changes, Colucci (1987) hypothesized that whether a block forms and what type of block forms (cyclonic vortex or anticyclonic vortex) appear to depend, respectively, on the amplitude of the existing planetary waves and on their phase relative to the cyclone. The mechanism coupling the surface cyclone with the planetary waves appears to be the advection of quasi-geostrophic potential vorticity by the 500 mb flow near the surface cyclone.

In spite of these studies supporting the positive effects of the synoptic-scale forcing on blocking, the rôle played by traveling cyclones in forcing a blocking episode is clouded by the fact that large-scale blocking is usually located in the region of decaying traveling cyclones. Though strong poleward momentum flux in the region of decaying storms was found by Blackmon et al. (1977), their results indicated that the low-level heat flux was stronger over the eastern coasts of the continents, where storms developed, than over the western continents. Blackmon and White (1982) suggested that the observed heat flux maximum in the upper troposphere is primarily associated with waves of larger spatial and longer temporal scales than those associated with baroclinic instability. The question arises whether the heat transport by the traveling cyclones leads to the warm anomalies of the block. The results of Mullen (1987) showed that the heat transports by the cyclone-scale eddies work to reduce the thermal perturbations of the fully developed block. He suggested that the primary mechanism responsible for maintaining the warmth of the block is the advection of time–mean temperature by the time–mean wind. However, Mullen (1987) noted that his investigation focused primarily on the fully developed block. The rôle of synoptic-scale transients in the initiation of the blocking may be different. Shutts (1983) suggested that the initiation of the relative warmth of the block might be maintained by the northward transport of warm subtropical air associated with dissipating transient cyclones. Utilizing a dry general circulation model with a mean thermal restoring force, Hayashi and Golder (1987) found that wave–wave interactions energetically play a more important rôle in the growth of ultralong waves than in their maintenance. Ultralong waves initially grow much more rapidly with wave–wave interactions than they do without these interactions. However, in their mature stage, these waves attain smaller amplitudes in the presence of higher wavenumbers than they do in their absence.

Though the pronounced influence of blocking on weather situations has received considerable attention, the dynamic picture of blocking is not yet clear. Holopainen and Fortelius (1987) pointed out that one of the reasons for the lack of definite conclusions from diagnostic studies perhaps has been the lack of suitable techniques for illustrating the net dynamic effects of eddies and that it would appear meaningful to apply different techniques now available to obtain a better picture of blocking. The intent of this paper is to apply a recently described diagnostic tool to study the net impact of eddy circulations during the initiation of an Atlantic blocking episode over southern Greenland on 21 January 1979. In this we hope to examine the importance of upstream explosive cyclogenesis and synoptic/planetary-scale interactions.

2. Methodology

2.1. Height tendency diagnoses

Height tendencies solved from the extended height tendency equation (Tsou et al., 1987; Smith and Tsou, 1988; Pauley and Smith, 1988) have been adopted to diagnose the basic mechanisms responsible for the Atlantic block formation. A general form of height tendency equation with hydrostatic balance as the only assumption can be expressed as (Tsou et al., 1987)

$$\underbrace{\left[\nabla^2 + \frac{(\zeta+f)f}{\sigma}\frac{\partial^2}{\partial p^2}\right]\frac{\partial \phi}{\partial t}}_{(A)} \underbrace{- \frac{1}{f}\nabla f\cdot\nabla\frac{\partial \phi}{\partial t}}_{(A')} \underbrace{+ f\frac{\partial \zeta_{ag}}{\partial t}}_{(A'')}$$

$$= \underbrace{-f\boldsymbol{V}\cdot\nabla(\zeta+f)}_{(B)} \underbrace{+ \frac{(\zeta+f)fR}{\sigma}\frac{\partial}{\partial p}\left(\boldsymbol{V}\cdot\nabla\frac{T}{p}\right)}_{(C)}$$

$$\underbrace{-\frac{(\zeta+f)fR}{\sigma c_p}\frac{\partial}{\partial p}\left(\frac{\dot{q}}{p}\right)}_{(D)} \underbrace{- \frac{(\zeta+f)f}{\sigma}\omega\frac{\partial \sigma}{\partial p}}_{(E)}$$

$$\underbrace{-f\left(\frac{\partial \omega}{\partial x}\frac{\partial v}{\partial p} - \frac{\partial \omega}{\partial y}\frac{\partial u}{\partial p}\right)}_{(F)} \underbrace{- f\omega\frac{\partial \zeta}{\partial p}}_{(G)}$$

$$\underbrace{+ f\boldsymbol{k}\cdot\nabla\times\boldsymbol{F}}_{(H)}, \tag{1}$$

where $\sigma = -RT/P\theta(\partial\theta/\partial P)$ is the static stability parameter; ζ the vertical component of relative vorticity; f the coriolis parameter; $\boldsymbol{V}$ the horizontal wind vector; ω the vertical motion in isobaric coordinates; $\dot{q}$ the diabatic heating rate; ϕ the geopotential; T the temperature; θ the potential temperature; c_p the specific heat of dry air at constant pressure; R the dry air gas constant; $\boldsymbol{F}$ the frictional force; and ∇ the horizontal del operator on an isobaric surface. Height (z) enters (1) through $\phi = gz$, where $g = 9.8$ m s^{-2}.

The forcing components on the right-hand-side of (1) are horizontal vorticity advection (term B), vertically differential horizontal thermal advection (term C), vertically differential heating (term D), vertical advection of static stability (term E), tilting effects (term F), vertical advection of vorticity (term G), and frictional effects (term H). The left-hand-side components of (1) are the Laplacian of the geopotential tendency (term A), β term (term A'), and ageostrophic vorticity tendency (term A''). A scale analysis from Tsou et al. (1987) for all terms in (1) except (H) is shown in Table 1. For the 3 Rossby number (R_o) values, 0.1, 0.25, and 0.5, A' is negligible and F and G are small. Also, the contributions of terms A'' and B through G to the height tendency were calculated using the present data set as a further check on the scale analysis. H was neglected in these calculations since the impact of H on the height changes at and above 500 mb was perceived to be small. Clearly, this assumption would be less appropriate for tendency calculations near the lower boundary. The results revealed that height tendency fields forced by F and G are much smaller than those forced by other terms, thus confirming the scale analysis. In addition, their effects were opposite to each other. Thus, F and G are not discussed in the following analyses. The height tendency fields forced by ageostrophic vorticity tendency were not generally small enough to be neglected. However, this effect did not alter the general behavior of the height tendency fields. In general, height tendency patterns with and without ageostrophic vorticity tendency were very similar. In addition, 48-h area mean absolute values for the whole domain were almost identical. Further, although suitable for general considerations, the uncertainties in calculations of term A'' preclude its inclusion in precise synoptic analyses. Thus, based on the scale analysis and the experimental calculations, (1) was simplified to the following equation:

Table 1. *Scale analysis of terms in (1) using characteristic values from Tsou et al. (1987)* (s^{-3})

	R_o		
Term	0.10	0.25	0.50
A	1×10^{-14}	8×10^{-14}	4.0×10^{-13}
A'	1×10^{-15}	6×10^{-15}	2.5×10^{-14}
A''	1×10^{-15}	2×10^{-14}	1.0×10^{-13}
B	1×10^{-14}	6×10^{-14}	2.5×10^{-13}
C	1×10^{-14}	7×10^{-14}	3.0×10^{-13}
D	1×10^{-14}	6×10^{-14}	1.5×10^{-13}
E	1×10^{-14}	8×10^{-14}	2.0×10^{-13}
F	1×10^{-15}	2×10^{-14}	6.0×10^{-14}
G	1×10^{-15}	2×10^{-14}	6.0×10^{-14}

$$\left[\nabla^2 + \frac{(\zeta+f)f}{\sigma}\frac{\partial^2}{\partial p^2}\right]\frac{\partial\phi}{\partial t} = -f\boldsymbol{V}\cdot\nabla(\zeta+f) + \frac{(\zeta+f)fR}{\sigma}\frac{\partial}{\partial p}\left(\boldsymbol{V}\cdot\nabla\frac{T}{p}\right) - \frac{(\zeta+f)f}{\sigma}\frac{R}{c_p}\frac{\partial}{\partial p}\left(\frac{\dot{q}}{p}\right) - \frac{(\zeta+f)f}{\sigma}\omega\frac{\partial\sigma}{\partial p}, \qquad (2)$$

identified by Tsou et al. (1987) as the extended height tendency equation. Note that (2) preserves the simplicity of the familiar quasi-geostrophic form of the height tendency equation, but replaces the geostrophic wind and relative vorticity by the observed value. Thus, the ageostrophic vorticity and temperature advection, which might be significant during the formation of the block and the upstream cyclones, are included. Also included are strong diabatic heating, and three-dimensionally varying static stability. More detailed discussions of (2) can be found in Tsou et al. (1987), Pauley and Smith (1988), and Smith and Tsou (1988).

The data set used was the SOP-1 FGGE level III-b analyses (Baker, 1983) obtained from the Goddard Laboratory for Atmospheres (GLA), described in the next section. Using these data, height tendencies were solved using successive over-relaxation with zero boundary conditions at the lateral boundaries. At the upper (100 mb) and lower (first pressure level above the surface) boundaries, the vertical derivatives of height tendency were assumed to be zero, i.e.,

$$\frac{\partial}{\partial p}\left(\frac{\partial \phi}{\partial t}\right)=0 \quad \text{at the upper and lower boundaries.}$$

The lower and upper boundary conditions are based on the thermodynamic energy equation. In this study since the diabatic heating and vertical velocity are assumed to be zero at these two boundaries, the horizontal temperature advection must also be assumed to be zero at these two boundaries in order to provide thermodynamic balance. Tests were also conducted to assess the impact of using non-zero horizontal temperature advections at the lower boundary, the approach used by Lau and Holopainen (1984). Results showed that the differences between height tendencies solved with the two lower boundary conditions decreased with decreasing height. These differences were negligible at 500 mb over the ridge area. Thus, the simpler zero advection boundary condition was used here. Eq. (2) was also solved for the height tendency associated with each of the right-hand-side forcing terms individually. In this case only the boundary condition associated with each individual term was used in the computations.

The solution of the height tendency equation requires that it be elliptic. In order to ensure that ellipticity is maintained, both σ and $(\zeta + f)$ were forced to be positive. For σ, the lapse rate was not allowed to be greater than 9°C/km. If after σ was adjusted, the total coefficient $f(f+\zeta)/\sigma$ was still negative, then the coefficient was set to be a small positive value about one percent of the area average value of the coefficient f^2/σ. The horizontal and vertical derivatives on both sides of the height tendency equation were approximated by the second-order, central difference scheme. The relaxation iteration was terminated when the absolute difference between two successive solutions of geopotential tendency was less than $10^{-4}\ \mathrm{m^2\,s^{-3}}$, corresponding to a height change of 0.4 m in 12 h, for all grid points.

Vertical motions required in these calculations were solved from the form of the omega equation corresponding to (2), namely,

$$\nabla^2 \sigma\omega + f(f+\zeta)\frac{\partial^2 \omega}{\partial p^2} = f\frac{\partial}{\partial p}[\boldsymbol{V}\cdot\nabla(\zeta+f)] + \frac{R}{p}\nabla^2(\boldsymbol{V}\cdot\nabla T) - \frac{R}{c_p p}\nabla^2 \dot{q}. \quad (3)$$

The only diabatic heating effect included in the ω calculation was the latent heating obtained from the GLA analyses. The simulated latent heat release of the GLA model contains two parts, large-scale and sub-grid scale convection. Large-scale precipitation occurs at a particular level when the specific humidity at that level exceeds the saturation value. It terminates when the relative humidity is reduced to 100% through the loss of condensed water. The moisture released by this process is assumed to evaporate into the next unsaturated layer or to precipitate if all lower layers are saturated. The small-scale cumulus parameterization scheme of the GLA model is a modification of the Arakawa's scheme for the UCLA 3-level model (Arakawa, 1972). There are 3 types of convection simulated by this parameterization: (1) middle-level convection; (2) penetrating convection; (3) low-level convection. A detailed description of the latent heating schemes can be found in Kalnay et al. (1983).

2.2. *Scale partitioning*

An intense cyclone which developed prior to the initiation of the Atlantic block under investigation in this study occurred directly upstream of the developing ridge (Figs. 3, 4). Recognizing the close relationship between the synoptic-scale flow and the blocking ridge, it is natural to hypothesize that the cyclone wave forcing was important to the formation of the Atlantic block. The importance of synoptic-scale features and their interaction with the block are diagnosed using the extended height tendency equation with forcing processes partitioned into planetary-scale, synoptic-scale, and scale interaction components. Most approaches to decompose the flow into different wavelengths are based on spectral methods over hemispheric or global domains. However, Gall et al. (1979) suggested that using Fourier series on the whole latitude belt to study the impact of cyclone waves on ultralong waves might be inappropriate, since the development of cyclone waves is essentially a local process. Thus, the Barnes (1964) objective analysis procedure is adopted to decompose the flow into synoptic and planetary-scale components in a limited domain. This filtering technique sacrifices the orthogonality property of the spectral technique; however, the local effects of synoptic-scale forcing on the planetary-scale

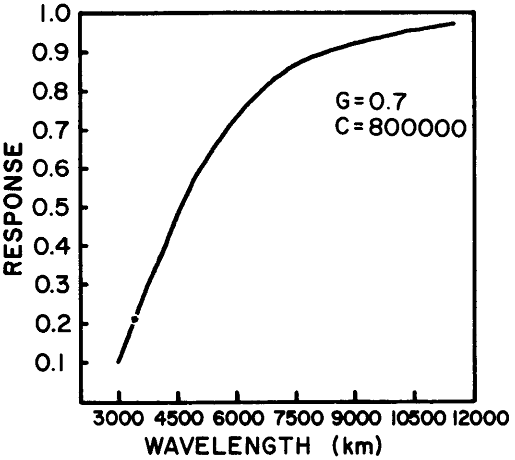

Fig. 1. Response curve used for the Barnes objective analysis scheme.

waves in the regional area can be accessed by this technique. The planetary-scale component is represented by the filtered field obtained from the Barnes scheme. The difference between the planetary-scale component and the original analyzed field is defined as the synoptic-scale component. One advantage of the Barnes objective analysis is that the weighted function constants are chosen prior to the analysis so that desired scale resolution can be determined prior to the analysis. Subjective investigation of 500 mb height fields has revealed the preferred scale of the block to be 5000–6000 km and the synoptic waves to be 1500–3000 km. Thus, filter constants were chosen to yield a response function which retains 73% of the signal at 6000 km and only 11% at 3000 km. The response curve is shown in Fig. 1.

To utilize the partitioned flow components, a partitioned form of (2) was formulated. This equation can be obtained by the following procedure. First, replace the right-hand-side variables in the vorticity and thermodynamic equations with the sum of their planetary-scale and synoptic-scale components. Second, follow the procedure made in deriving (1). Finally, apply the approximations made in deriving (2). The resulting equation is

$$\left[\nabla^2 + \frac{(\zeta+f)f}{\sigma}\frac{\partial^2}{\partial p^2}\right]\frac{\partial \phi}{\partial t} = P + S + SP, \tag{4}$$

where

P = the planetary-scale forcing

$$= -f\tilde{V}\cdot\nabla(\tilde{\zeta}+f) + \frac{(\zeta+f)fR}{\sigma}\frac{\partial}{\partial p}(\tilde{V}\cdot\nabla\tilde{T}) - \frac{(\zeta+f)f}{\sigma}\frac{R}{c_p}\frac{\partial}{\partial p}\left(\frac{\tilde{\dot{q}}}{p}\right) - \frac{(\zeta+f)f}{\sigma}\tilde{\omega}\frac{\partial\tilde{\sigma}}{\partial p};$$

S = the synoptic-scale forcing

$$= -fV^*\cdot\nabla(\zeta^*+f) + \frac{(\zeta+f)fR}{\sigma}\frac{\partial}{\partial p}(V^*\cdot\nabla T^*) - \frac{(\zeta+f)f}{\sigma}\frac{R}{c_p}\frac{\partial}{\partial p}\left(\frac{\dot{q}^*}{p}\right) - \frac{(\zeta+f)f}{\sigma}\omega^*\frac{\partial\sigma^*}{\partial p};$$

SP = the scale-interaction forcing

$$= -f(\tilde{V}\cdot\nabla\zeta^* + V^*\cdot\nabla\tilde{\zeta}) + \frac{(\zeta+f)fR}{\sigma}\frac{\partial}{\partial p}(\tilde{V}\cdot\nabla T^* + V^*\cdot\nabla\tilde{T}) - \frac{(\zeta+f)f}{\sigma}\left(\tilde{\omega}\frac{\partial\sigma^*}{\partial p} + \omega^*\frac{\partial\tilde{\sigma}}{\partial p}\right),$$

where ($\tilde{}$) represents the planetary-scale and ( )* the synoptic-scale variables.

3. Data and synoptic discussion

3.1. Data

The data set used in this study is based on the SOP-1 FGGE III-b analyses obtained from the Goddard Laboratory for Atmospheres (GLA). The objective analysis procedure developed at the GLA is a successive correction method of the Cressman (1959) type, but modified to include variable data density and quality. Eastward and northward wind components u and v, geopotential height, and relative humidity are analyzed on mandatory pressure levels. Surface pressure and temperature are reduced to sea level and analyzed there. The analyzed data were then compared with the model first guess fields interpolated from sigma levels. The assimilation/forecast model utilized for data analysis is the global fourth-order version of the GLA General Circulation Model (GCM). This model is based on an energy conserving scheme with all horizontal differences computed with fourth-order accuracy. There are

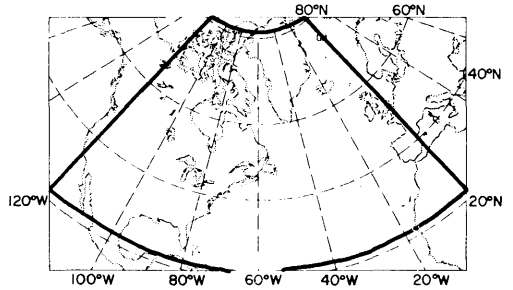

Fig. 2. Geographic location of the horizontal computational domain (area inside the heavy solid line).

nine layers in vertical sigma coordinates with a uniform non-staggered horizontal grid (4° latitude by 5° longitude). Detailed descriptions of the model can be found in Kalnay-Rivas et al. (1977). The model first guess fields were updated every 6 h at the model sigma levels.

After the comparison is made between the data and the model first guess fields interpolated to constant pressure levels, observational data are rejected if their difference between the model first guess fields are more than specified limits (Baker, 1983, his Table 2) of the average difference between the nearby reports (observations within a 5° radius) and the model first guess fields. To minimize the error introduced by vertical interpolation between sigma and pressure, the differences between the model first guess and the analyzed fields are interpolated back to the sigma levels. The new initialized sigma level fields for the next 6 h model forecast are the sum of the original model fields and the differences between the analyzed data and the model first guess fields. Detailed descriptions of data manipulation can be found in Baker (1983).

To focus on the Atlantic block and its upstream cyclone, only a portion of the original global data set, covering a domain from 0° to 120° W and 22° to 82° N (Fig. 2) during the period 17–21 January 1979, was selected for analysis in this study. In addition, the mandatory level data (4° latitude by 5° longitude) were interpolated or extrapolated to standard isobaric surfaces from 1050 mb to 50 mb in 50 mb increments. The vertical interpolation technique used was the same as described in Baker (1983) in order to be consistent with the original data manipulation.

3.2. Synoptic discussion

The evolution of the block formation at 500 mb and the development of the upstream cyclone are depicted in Figs. 3, 4. It is interesting to note that this planetary-scale block did not originate as a stationary planetary-scale ridge, nor did it appear to be a retrogression of a pre-existing block that was present over the eastern Atlantic Ocean on 14 January. Rather it developed quite independently from an eastward propagating short-wave ridge. Its development is closely related to an upstream surface cyclone that originated over Lake Michigan at 1200 GMT 17 January. In the initial 24-h period, the short-wave ridge migrated eastward with the surface cyclone without significantly changing its amplitude. The amplitude of the ridge began to grow and its speed decreased as the eastward propagating cyclone center passed the New England shore and began developing explosively at 1200 GMT 18 January. By 0000 GMT 20 January the slow-moving ridge became stationary and began to build northward. This occurred 12 h after the cyclone reached its minimum sea level pressure (SLP) of 971 mb. The SLP of the cyclone dramatically decreased during the entire 24-h period prior to this time. In particular, the central SLP of the cyclone dropped by 28 mb during the 18 h from 1200 GMT on the 18th to 0600 GMT on the 19th (Fig. 5). Notice that the eastward movement of the surface cyclone was hindered by the developing ridge and the surface cyclone began to move northeastward at 1200 GMT 19 January. Over the remaining 36 h displayed, the ridge continued to build northward. Accompanying this amplification of the ridge was strong warm air transport which gradually warmed the air at the northern extent of the ridge. In addition, strong height gradients progressed from south to east of the low upstream from the ridge. Associated with these strong height gradients an isolated region of strong winds occurred west of the ridge at 300 mb (Fig. 6). A warm high at 500 mb first appeared on 0000 GMT 21 January southeast of southern Greenland, followed 12 h later by the formation of the block over southern Greenland. This block persisted through 27 January (not shown). The developing ridge further hindered the eastward movement of the surface cyclone and forced it to move northward or pause. The cyclone dramatically filled by 9 mb as it paused

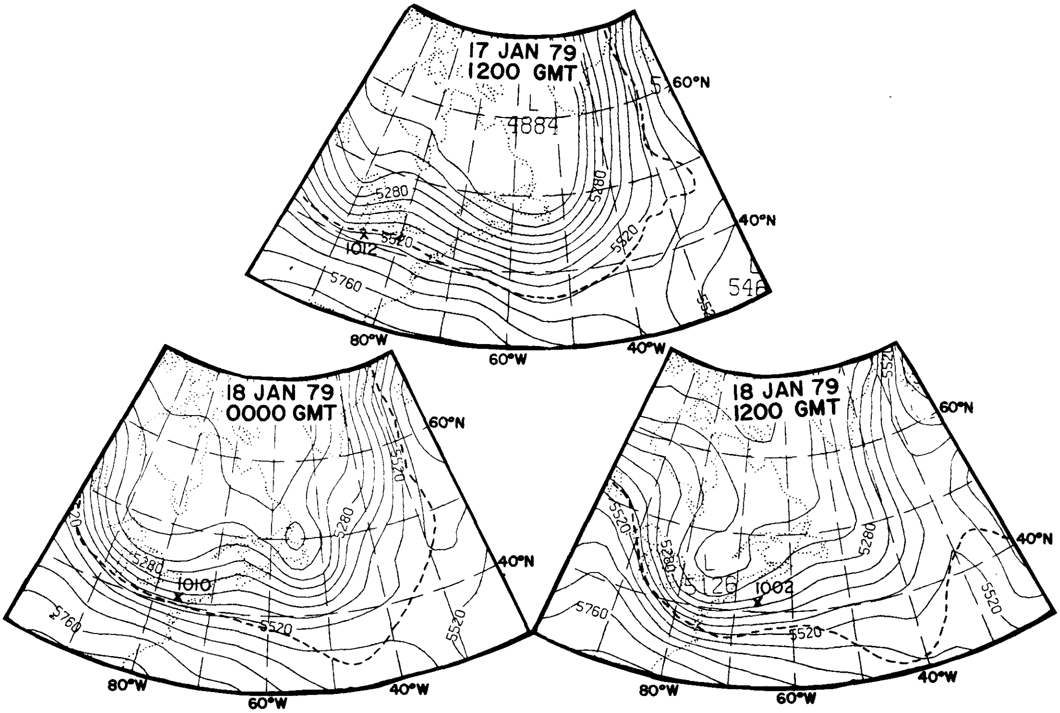

Fig. 3. 500 mb heights (solid, m, $\Delta Z = 60$ m) and 250°K isotherm (dashed) for 1200 GMT 17 January through 1200 GMT 18 January 1979. " × " represents the location of the surface cyclone with sea level pressure (SLP) indicated in mb.

from 1200 GMT 20 January to 0000 GMT 21 January.

Fig. 6 shows in 24-h intervals the evolving 300 mb height fields and isotachs. At 1200 GMT 17 January, when the surface low first appeared, two broad jet streak regions can be found on the west and east side of the long-wave trough over the Atlantic Ocean. A short-wave ridge was located east of the Great Lakes upstream from the long-wave trough in the region of strong winds. 24 h later, the jet streak on the east-side of the long wave trough propagated northward, while the jet streak on the west-side of the long-wave trough curved with the deepening low upstream from the ridge. By 1200 GMT 19 January, the former propagated out the domain displayed and the latter continued to propagate eastward with the deepening low. The amplitude of the ridge grew as the upstream low deepened. The evolution of the ridge development at 300 mb was very similar to that at 500 mb. By 1200 GMT 20 January, the ridge was well-developed and had become stationary. An isolated jet streak formed between the well-developed ridge and its upstream low, and 24 h later the block formed over southern Greenland.

To show the effect of the filtering procedure, partitioned synoptic-scale and planetary-scale height fields at 0000 GMT 20 January are depicted in Fig. 7. This map time is singled out here and later in the paper because it corresponds to the time that the ridge feature of interest became stationary and began building northward. Of particular interest are the proximity of the synoptic-scale and planetary-scale wave features over the Atlantic, signally the potential for strong scale interaction.

4. Height tendency results

Figs. 8–10 show the 500 mb height tendencies attributed to the total combined forcing and each individual forcing term in (2), except D, for 3

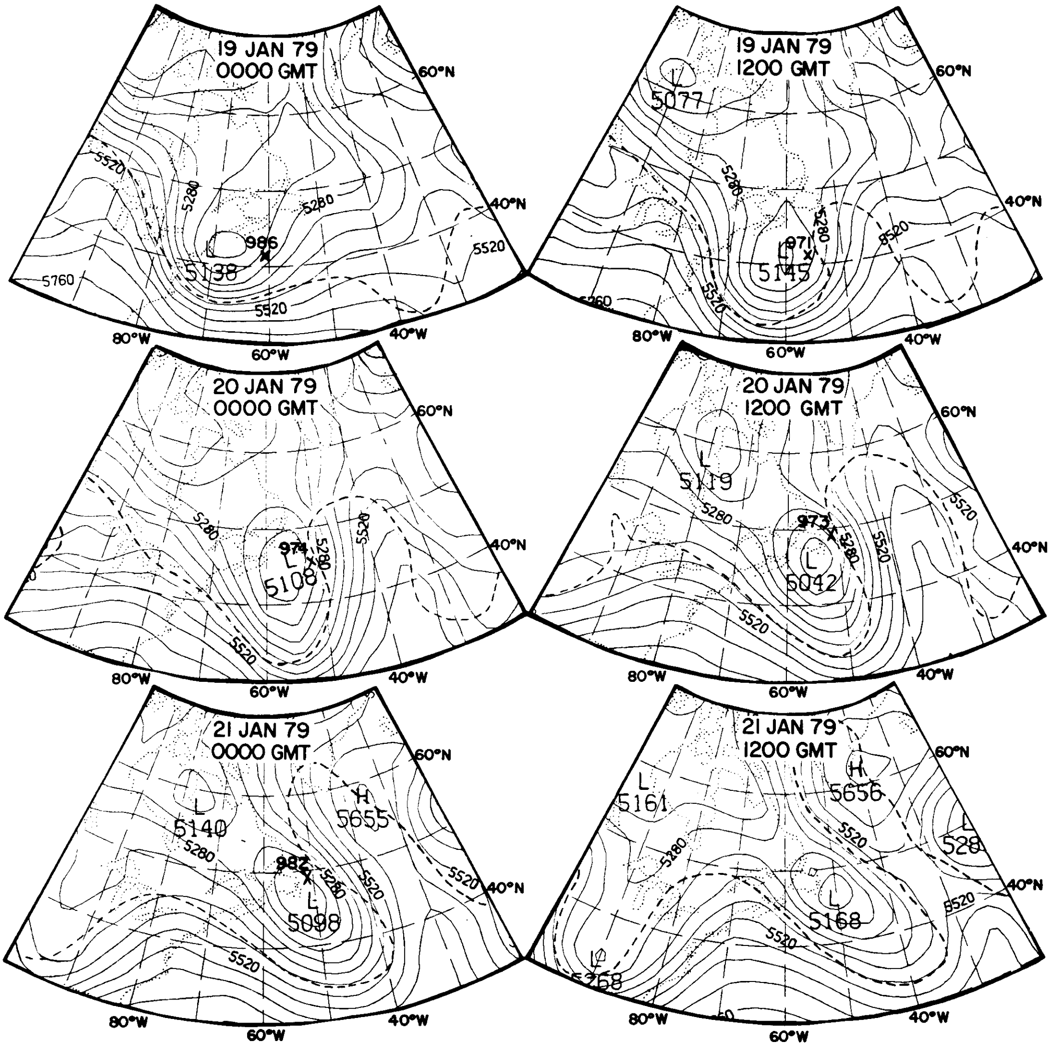

Fig. 4. As in Fig. 3 for the period from 0000 GMT 19 January through 1200 GMT 21 January 1979.

map times in 24-h intervals centered at the time 0000 GMT 20 January, when the ridge became stationary. In order to investigate the influence of height tendencies on the ridge development, height fields are superimposed on the tendency maps. Height tendencies attributed to the latent heating effect are not included in these diagnoses for two reasons. First, experimental calculations show that latent heating had little direct impact on the height changes at and above 500 mb. Second, almost no precipitation can be detected over the ridge and block area from satellite pictures; thus, the direct impact of latent heating on the formation of the block is small. Because of our interest in the developing ridge, the following discussion focusses on tendencies associated with that feature.

At 0000 GMT 19 January, height rises are seen along and downstream from the ridge (Fig. 8). This height change distribution suggests that the ridge should propagate eastward and intensify, behavior that is verified 24 h later (Fig. 9). Both

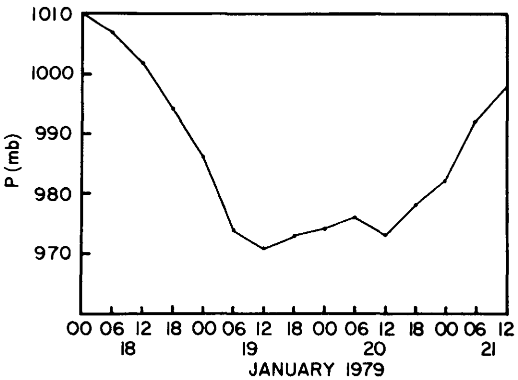

Fig. 5. Cyclone central SLP in mb.

the vorticity advection and vertically differential thermal advection made important contributions to the height rise region, although the vorticity advection contributions were larger. Acting opposite to the vorticity and thermal advection, the static stability advection forced height falls over the ridge area. This tendency to inhibit the growth and propagation of the ridge occurs in the presence of adiabatic warming associated with subsiding air. As pointed out by Smith and Tsou (1988), in an adiabatically warmed environment in which σ increases with decreasing pressure, the isobaric layer above a given level (500 mb in this case) will expand more than the layer below the level, resulting in a downward displacement of the level.

By 0000 GMT 20 January (Fig. 9), a broad region of significant height rises occurred along the ridge line and on the northern extent of the ridge. This suggests that we should expect the ridge to build northward and broaden its east–west extent, features verified in Fig. 10. Again, the total height rises were primarily forced by vorticity advection, with the rôle of differential thermal advection greatly reduced compared with the previous 24 h. Green (1977) proposed that the transfer of momentum by eddy motion could maintain blocking anticyclones. The present study shows that the vorticity advection was also important to the formation of the block. It is interesting to note that despite the strong northward warm air transport ahead of the cyclone (Fig. 4), vertically differential thermal advection did not significantly alter the height fields over the ridge area. Thus, although strong warm advection acts to increase the thickness of the height fields, the small vertical gradient in the advection results in only minor height rises. Note, however, that in the height fall region associated with the upstream cyclone the thermal advection contribution was comparable to the vorticity advection. This feature can also be identified 12 h earlier (not shown), when the SLP of surface cyclone reached minimum value. One of the rôles played by the differential thermal advection in this study was to maintain the intensity of the cyclone at 500 mb as it matured. This in turn indirectly influenced the downstream ridge through the synoptic-scale and synoptic/planetary-scale interaction forcing described in Section 5.

Once again, the static instability advection worked as a brake to inhibit the growth of the ridge, but its influence was not strong enough to offset the combined effects of vorticity and thermal advection. Thus, the ridge continued to grow northward and a closed high first appeared, at 0000 GMT 21 January (Fig. 10). As the closed high appeared, the magnitude of the total height tendencies decreased. The maximum height rises associated with the ridge occurred north and northwest of the high, while the height change in the center of the high was small. Such height tendency distributions would indicate that the high should propagate northwestward without notable intensification. Synoptic patterns (Fig. 4) show that the high retrograded without notable intensification during the succeeding 12-h period. Examining the height tendencies due to the individual forcing, it is obvious that all three forcing contributions to the height change decreased in magnitude. The vorticity advection was still the dominant forcing process, while the differential thermal advection and static stability advection forcing were small in the vicinity of the high.

The time evolution of each individual forcing term is summarized in Fig. 11 using area average statistics. The absolute value of tendencies was chosen for the averaging statistics, since we are interested in how vigorous the height changes were. The sensitivity of the area average calculations was tested by averaging the absolute tendencies over several different box sizes. Subjective analyses of the average results and height tendency fields show that the average

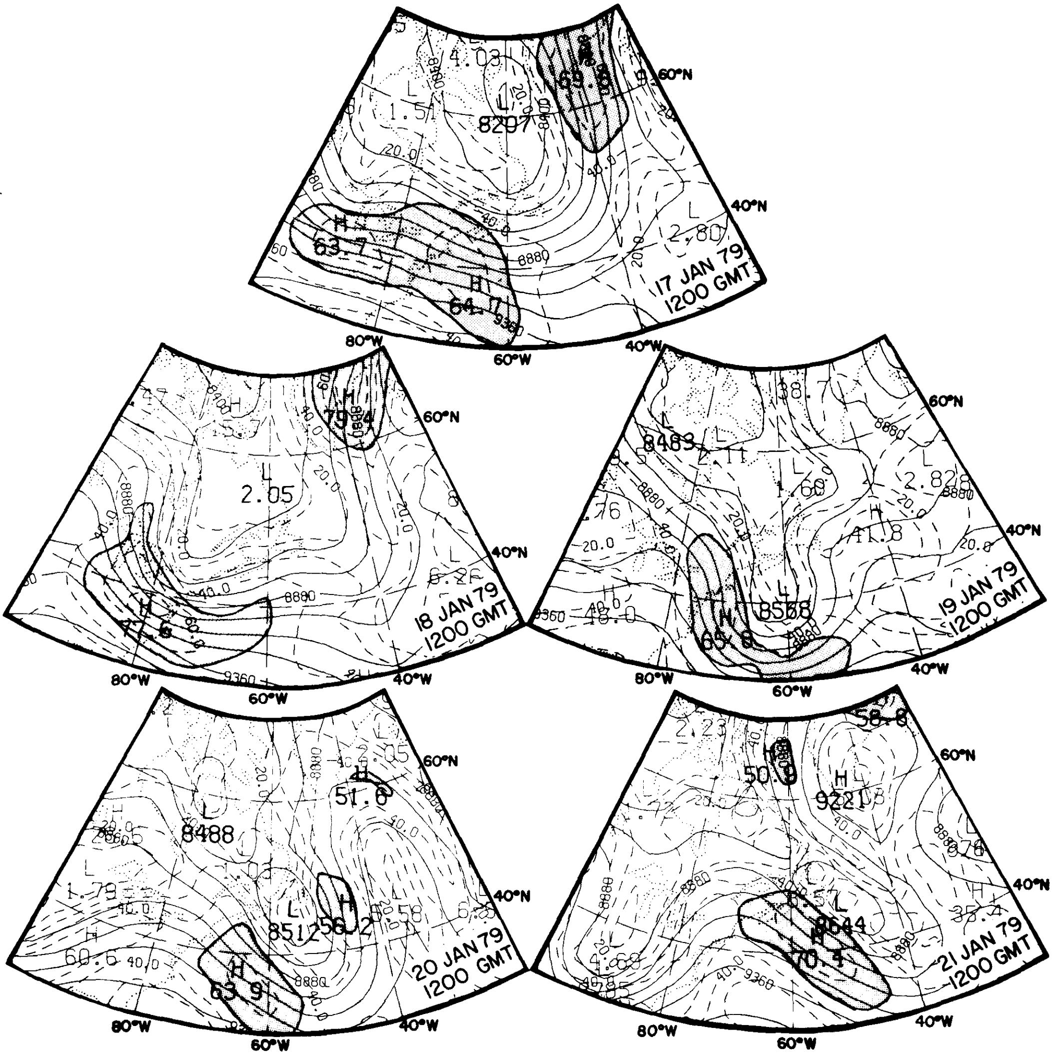

Fig. 6. 300 mb heights (solid, m, $\Delta Z = 120$ m) and isotachs (dashed, m s^{-1}, $\Delta V = 10$ m s^{-1}). Shaded areas encompass regions of wind speed greater than or equal to 50 m s^{-1}.

statistic most representative of the characteristics of the ridge development and block formation is the one averaged over the box which extends one grid point from the center of the maximum total height rise region. Examples of averaging boxes, which include nine grid points, are shown in Figs. 8–10.

It is apparent in Fig. 11 that the vorticity advection played the dominant rôle in the development of the ridge and the formation of block. However, initially, the effect of differential thermal advection was comparable or even greater than the vorticity advection. The change in this situation was primarily due to the dramatic increase of vorticity advection at 0000 GMT 19 January, 12 h after the cyclone began explosive development. It reached maximum intensity at 0000 GMT 20 January as the ridge became stationary. Throughout the period the braking effect of static stability advection was

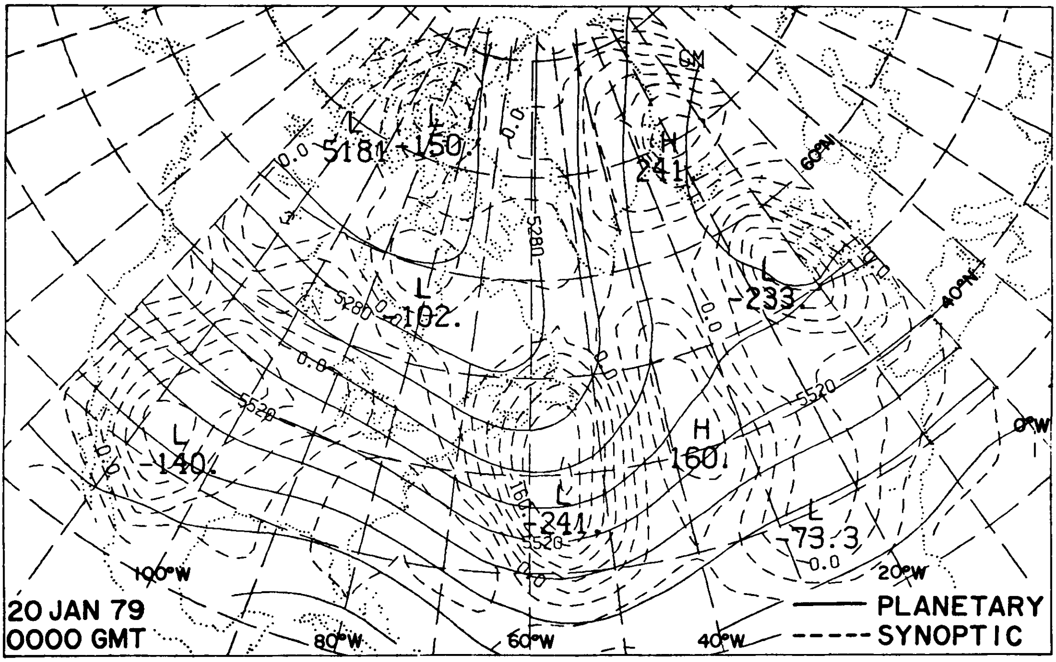

Fig. 7. 500 mb partitioned height fields (m) for planetary-scale (solid) and synoptic-scale (dashed) components at 0000 GMT 20 January.

not sufficient to compensate the combined effect of vorticity and differential thermal advection. This was especially true during the period from 0000 GMT 19 January to 1200 GMT 20 January. After the closed high appeared at 0000 GMT 21 January, all three forcing terms decreased in magnitude.

Since the vorticity advection was the dominant forcing process during the ridge development, its effect on the development of the ridge is further examined by separating the absolute vorticity advection into earth and relative vorticity advection components. Fig. 12 shows the height tendency fields attributed to these two forcing processes at 0000 GMT 20 January, when the vorticity advection reached its maximum value. The height rises attributed to the earth vorticity advection are seen in a broad region between the trough and ridge. This distribution indicates that the main effect of earth vorticity advection was to encourage the ridge to propagate westward. The height rises on the northern extent of the ridge were primarily contributed by the advection of anticyclonic relative vorticity. This implies that the relative vorticity minimum established on the anticyclonic side of the jet streak was favorable for the subsequent development of the ridge. This jet development and the subsequent vorticity advection identifies an important rôle of the upstream cyclone in the blocking development.

5. Partitioned tendencies results

Height tendency fields attributed to the planetary-scale, synoptic-scale, and planetary/synoptic-scale interaction forcing at 0000 GMT 20 January are shown in Fig. 13. The significant height rises at the northern extent of the ridge were primarily forced by synoptic/planetary-scale interactions. The synoptic-scale forcing assisted the intensification of the ridge but was smaller. The maximum height rises due to the synoptic-scale forcing appeared upstream of the stationary ridge. This resembles the observational results of Illari (1984) and Mullen (1987), who noted that the anticyclonic eddy forcing due to synoptic-scale transients tend to be one-quarter wave-

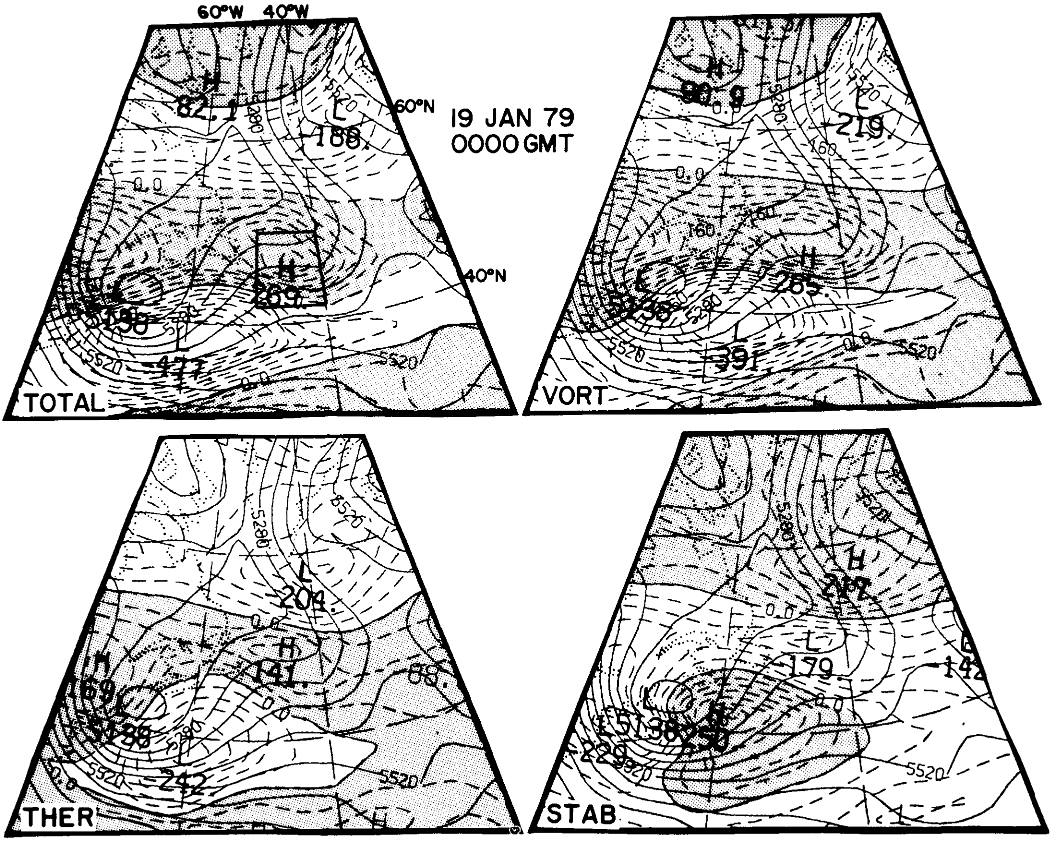

Fig. 8. Instantaneous height changes (m (12 h)$^{-1}$) attributed to the total and each individual forcing term in (2) for 0000 GMT 19 January. height rise areas shaded. Boxes represent averaging areas utilized in Figs. 11, 14, and 15.

length upstream of the block during the maintenance stage of the block. However, keep in mind that the scale-interaction forcing, which was not included in their studies, also played an important rôle during the growth of the stationary ridge. The main effect of the planetary-scale forcing was to encourage the ridge to propagate westward, since it primarily forced height rises on the west side of the ridge. The planetary-scale forcing contributed little to the northward building of the ridge. The northward and westward building of the ridge increased the zonal extents of the ridge and inhibited the eastward and northward movement of the surface cyclone. Thus, the surface cyclone began to decay 12 h later and a closed 500 mb high first appeared at 0000 GMT 21 January (Fig. 4).

To summarize the partitioned tendency results, the time evolution of the area mean absolute height changes due to the synoptic-scale, planetary-scale, and synoptic/planetary-scale interaction forcing are displayed in Fig. 14. Averaging areas are as specified for Figs. 8–10. The scale-interaction was dominant at the beginning of the study period. As explosive cyclone development began (1200 GMT 18 January) both synoptic-scale and scale-interaction forcing dramatically increased, while the planetary-scale forcing decreased. Of the two dominant forcing processes, the synoptic-scale was largest through the next 24 h, maximizing 6 h after the end of the explosive cyclone development period. Following this development and a concurrent return of the planetary-scale forcing to its original value, the inter-

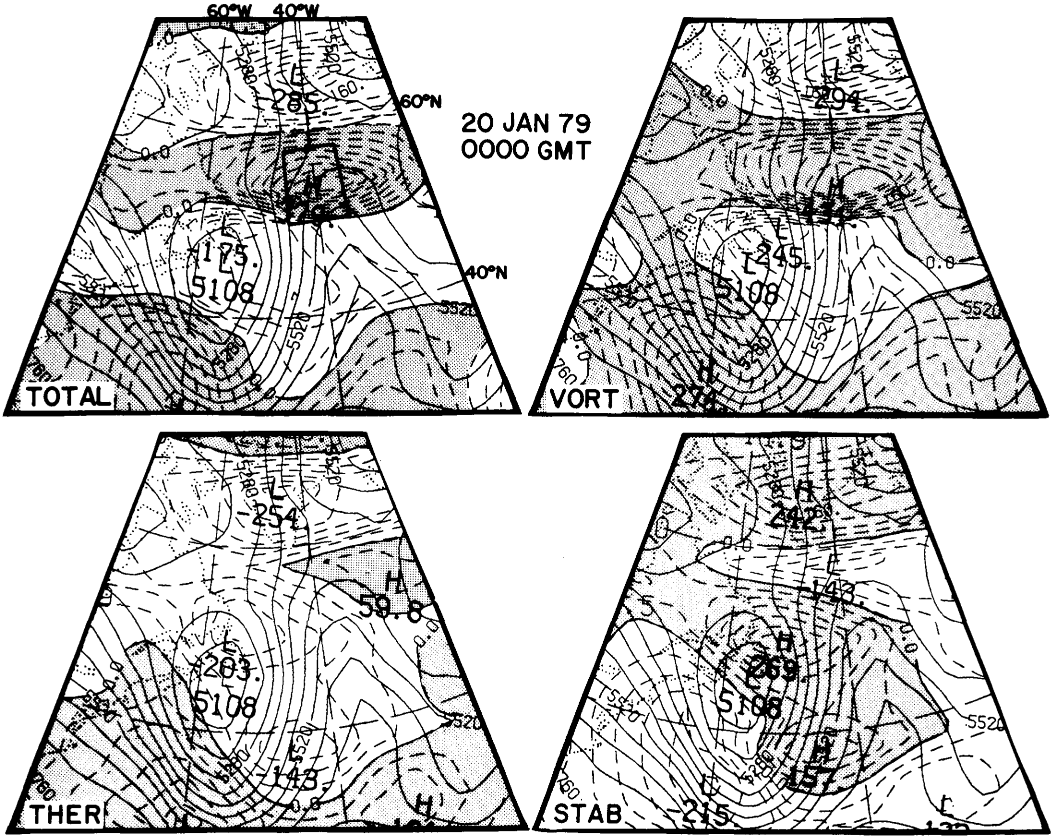

Fig. 9. As in Fig. 8 for 0000 GMT 20 January.

action forcing reached its peak intensity on 0000 GMT 20 January. The ensuing northward development of the ridge and initial block formation were dominated by scale-interaction processes, in agreement with the results of Hansen and Chen (1982) and Hansen (1986) that blocking features are dominated by non-linear interactions. This reflects the importance of the coupled synoptic-scale fields east of the upstream cyclone and the growing planetary-scale fields south of Greenland.

To further analyze the influence of each forcing component, Fig. 15 depicts the time evolution of mean absolute height changes due to the partitioned vorticity, thermal, and stability terms. In general, the major contribution to the vorticity advection was made by the scale-interaction component, with the synoptic-scale component playing a secondary rôle. Both the synoptic-scale and scale-interaction components dramatically increased at 0000 GMT 19 January, 12 h after explosive cyclone development began. The synoptic-scale forcing continued to increase and was greater than the scale-interaction forcing at 1200 GMT 19 January, when the SLP of the surface cyclone reached its minimum value. As the ridge became stationary at 0000 GMT 20 January, the scale-interaction reached maximum intensity, while the synoptic-scale component decreased. 12 h later, the scale-interaction component decreased as the surface cyclone began to decay. The planetary-scale component of vorticity advection remained small during the entire period of investigation.

Similar to the vorticity advection, the scale interaction was the dominant component of

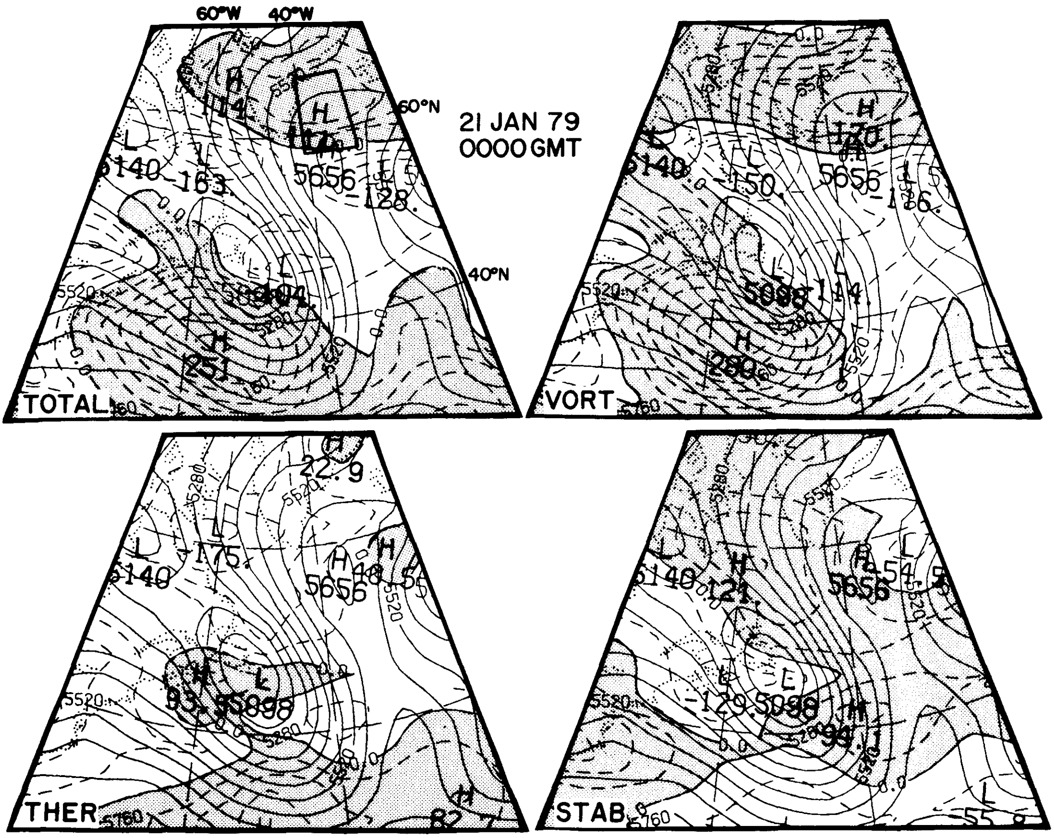

Fig. 10. As in Fig. 9 for 0000 GMT 21 January.

differential thermal advection during the first half of the investigation period. However, as the surface cyclone reached minimum SLP, the synoptic-scale and planetary-scale components became comparable to the scale-interaction component. Clearly, the dramatic increase in the scale-interaction and synoptic-scale components that occurred in the vorticity advection are not reflected in the thermal advection term. As a result the effect of differential thermal advection on the ridge development was much smaller than the vorticity advection (see Fig. 11).

The scale-interaction component also dominated the static stability advection and shows time variations similar to those seen in the vorticity advection. Such similarities did not occur in the other two components. In fact, the synoptic-scale component only increased slightly during explosive cyclone development, in contrast to the sharp increase noted in the vorticity advection terms. Since the static stability term generally opposes the vorticity and differential thermal advection, the net effect on the synoptic-scale component forcing was to produce a value greater than the scale-interaction forcing during this time (see Fig. 14).

In summary, the scale-interaction component of the vorticity and differential thermal advection played the primary rôle during the eastward movement of the migrating ridge. As the surface cyclone developed, both the synoptic and scale-interaction components of vorticity advection dominated the development of the ridge. By the time the surface cyclone began to decay and the ridge to build northward, the synoptic-scale component of vorticity advection dramatically decreased, while the scale-interaction component remained important to the formation of the block.

Finally, since the scale-interaction component of vorticity advection had such strong influence on the ridge development, it is of interest to examine the two parts of the scale-interaction component (see the expression for SP in (4)). This is presented for 0000 GMT 20 January in Fig. 16. It is obvious that the height tendency distribution was dominated by the advection of synoptic-scale vorticity by the planetary-scale wind. In fact, the advection of planetary-scale vorticity by the synoptic-scale wind actually produced height falls over the ridge area, thus inhibiting the growth of the block. These results further verify the importance of the jet streak and the corresponding anticyclonic vorticity maximum associated with the deepending upstream cyclone on the development of the ridge. However, they also indicate the importance of the proper phasing of the synoptic-scale vorticity with the planetary-scale wind field. This confirms Colucci's (1987) suggestion that the occurrence of blocks depends critically upon the amplitude of existing planetary-scale waves and their phase relationship with the upstream cyclones.

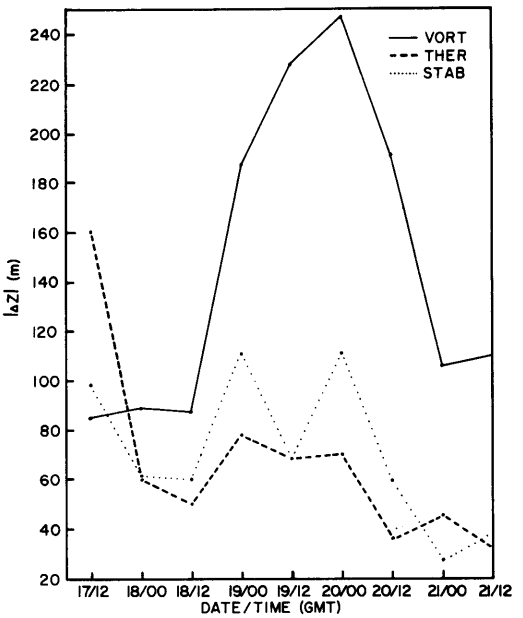

Fig. 11. Area mean absolute instantaneous height changes (m (12 h)$^{-1}$) attributed to each forcing term in (2). See Figs. 8–10 for averaging area examples.

6. Summary

An observational study has been conducted to investigate the development of a blocking anticyclone that first appeared on 21 January 1979 over the North Atlantic Ocean. The data set used is based on the FGGE-III b analyses

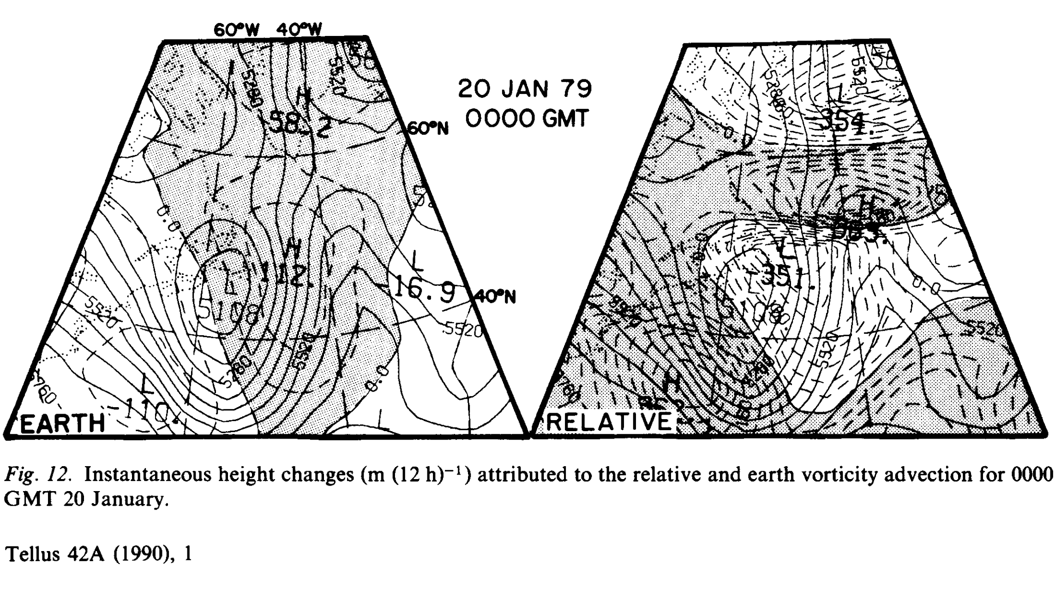

Fig. 12. Instantaneous height changes (m (12 h)$^{-1}$) attributed to the relative and earth vorticity advection for 0000 GMT 20 January.

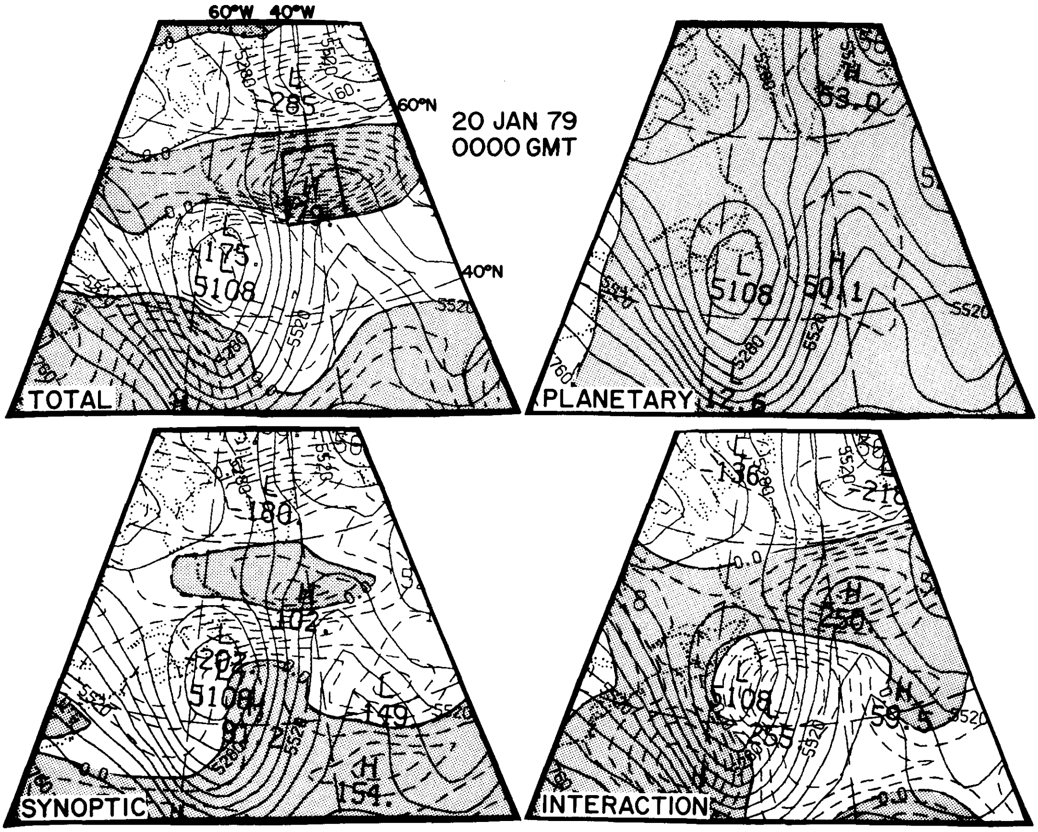

Fig. 13. Instantaneous height changes (m (12 h)$^{-1}$) attributed to the total and planetary-scale, synoptic-scale, and scale-interaction components in (4) for 0000 GMT 20 January 1979. Height rise areas shaded.

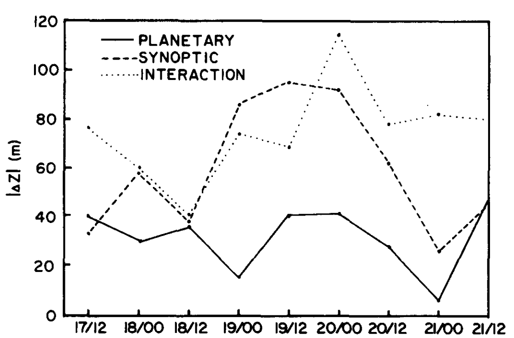

Fig. 14. Area mean absolute instantaneous height changes (m (12 h)$^{-1}$) due to each component in (4).

obtained from GLA (Baker, 1983). Height tendencies solved from the extended height tendency equation (Tsou et al., 1987) have been chosen as the primary diagnostic tool. The extended height tendency results show that the development of the ridge was closely related to an upstream cyclone that developed explosively prior to the block formation. To further analyze the importance of the cyclone and the corresponding synoptic/planetary-scale interactions, height tendencies were also solved from a partitioned form of the height tendency equation. Barnes' (1964) objective analysis scheme was adopted to decompose the flow into planetary and synoptic-scale components.

Height tendency results indicate that during the period of ridge propagation without significant amplification, both the vorticity and differential thermal advection were important forcing mechanisms. However, as the cyclone explosively developed, the vorticity advection dramatically increased and ultimately became the primary forcing processes for the development of the ridge. Further examination of the vorticity advection revealed that the northward building ridge was largely influenced by the advection of anticyclonic vorticity located on the anticyclonic side of a jet streak that became established on the east side of the upstream cyclone. The direct impact of differential thermal advection on the development of the ridge was much smaller than the vorticity advection during ridge amplification. However, its effect on the maintenance of the upstream cyclone was comparable to the vorticity advection. Thus, the thermal advection indirectly influenced the downstream ridge through the subsequent synoptic-scale and synoptic/planetary-scale interaction forcings. The main effect of static stability advection was to inhibit the propagation and growth of the ridge. However, it was not strong enough to offset the combined effect of vorticity and differential thermal advection.

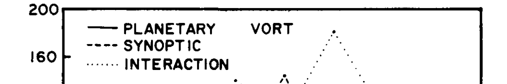

Fig. 15. Area mean absolute instantaneous height changes (m (12 h)$^{-1}$) attributed to each forcing term for partitioned components in (4).

In their partitioned form the height tendencies show that during the early ridge migration eastward the scale-interaction forcing was the largest of the three components and was significant in both the vorticity and differential thermal advection terms. Then once again the explosive cyclone development marked significant changes, with the effect of both the scale-interaction and synoptic-scale forcing dramatically increasing. The former primarily resulted from the dramatic increase of the scale-interaction component of the vorticity advection. The latter was caused by strong synoptic-scale vorticity advection and

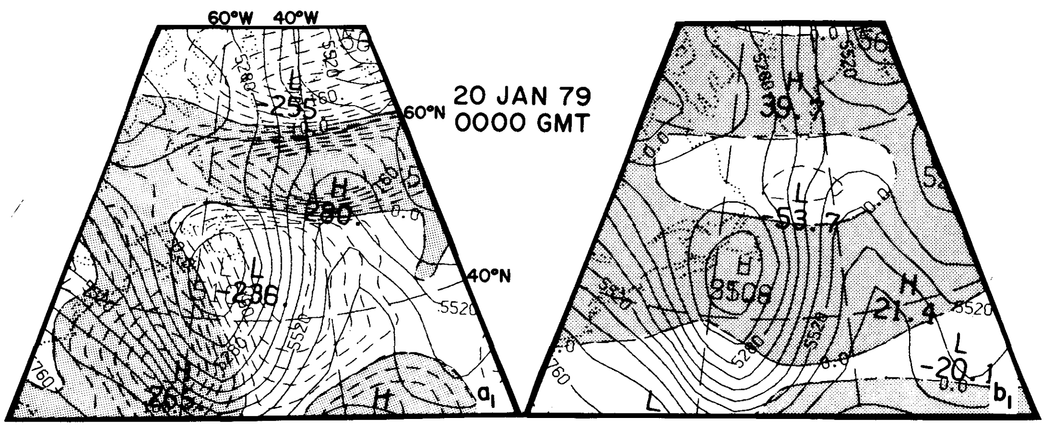

Fig. 16. Instantaneous height changes (m (12 h^{-1})) attributed to (a) advection of synoptic-scale vorticity by planetary-scale winds, and (b) advection of planetary-scale vorticity by synoptic-scale winds.

the weak inhibiting effect of synoptic-scale static stability advection. Synoptic-scale forcing reached its maximum value when the sea level pressure of the cyclone reached its minimum value. 12 h later, when the ridge became stationary, the scale-interaction forcing reached its maximum intensity and then continued to dominate throughout the block formation.

7. Acknowledgements

The authors are indebted to Richard Knabb for data tabulations and figure drafting and to the anonymous reviewers for their very helpful comments. This work was supported by the National Aeronautics and Space Administration under Contract NAS 834009.

REFERENCES

Arakawa, A. 1972. Design of the UCLA general circulation model. Tech. Rept. No. 7, *Numerical simulation of weather and climate*. Dept. of Meteorology, UCLA, 116 pp.

Austin, J. F. 1980. The blocking of middle latitude westerly winds by planetary waves. *Quart. J. Roy. Meteor. Soc. 106*, 327–350.

Baker, W. E. 1983. Objective analysis and assimilation of observational data from FGGE. *Mon. Wea. Rev. 111*, 328–342.

Barnes, S. L. 1964. A technique for maximizing details in numerical weather map analysis. *J. Appl. Meteor. 3*, 396–409.

Blackmon, M. L., Wallace, J. M., Lau, N.-C. and Mullen, S. L. 1977. An observational study of the Northern Hemisphere wintertime circulation. *J. Atmos. Sci. 34*, 1040–1053.

Blackmon, M. L. and White, G. H. 1982. Zonal wavenumber characteristics of Northern Hemisphere transient eddies. *J. Atmos. Sci. 39*, 1985–1998.

Cehelsky, P. and Tung, K. K. 1987. Theories of multiple equilibria and weather regimes—A critical reexamination. Part II: Baroclinic two-layer models. *J. Atmos. Sci. 44*, 3282–3303.

Charney, J. G. and DeVore, J. G. 1979. Multiple-flow equilibria in the atmosphere and blocking. *J. Atmos. Sci. 36*, 1157–1176.

Charney, J. G. and Straus, D. M. 1980. Form-drag instability, multiple equilibria and propagating planetary waves in baroclinic, orographically forced planetary wave systems. *J. Atmos. Sci. 37*, 1157–1176.

Charney, J. G., Shukla, J. and Mo, K. C. 1981. Comparison of a barotropic blocking theory with observation. *J. Atmos. Sci. 30*, 762–779.

Colucci, S. J. 1987. Comparative diagnosis of blocking versus nonblocking planetary-scale circulation changes during synoptic-scale cyclogenesis. *J. Atmos. Sci. 44*, 124–139.

Cressman, G. 1959. An operational objective analysis system. *Mon. Wea. Rev. 87*, 367–374.

Egger, J. 1978. Dynamics of blocking highs. *J. Atmos. Sci. 35*, 1788–1801.

Frederiksen, J. S. 1983. A unified three-dimensional instability theory of the onset of blocking and cyclogenesis. II. Teleconnection patterns. *J. Atmos. Sci. 40*, 2593–2609.

Gall, R., Blakeslee, R. and Somerville, R. C. J. 1979. Cyclone-scale forcing of ultralong waves. *J. Atmos. Sci. 36*, 1692–1698.

Green, J. S. A. 1977. The weather during July 1976: Some dynamic considerations of the drought. *Weather 32*, 120–126.

Hansen, A. R. 1986. Observational characteristics of atmospheric planetary waves with bimodal amplitude distribution. *Adv. Geophys. 29*, 101–133.

Hansen, A. R. and Chen, T.-C. 1982. A spectral energetics analysis of atmospheric blocking. *Mon. Wea. Rev. 110*, 1146–1165.

Hayashi, Y. and Golder, D. G. 1987. Effects of wave–wave and wave–mean flow interactions on the growth and maintenance of transient planetary waves in the presence of a mean thermal restoring force. *J. Atmos. Sci. 44*, 3392–3401.

Holopainen, E. and Fortelius, C. 1987. High frequency transient eddies and blocking. *J. Atmos. Sci. 44*, 1632–1645.

Illari, L. 1984. A diagnostic study of the potential vorticity in a warm blocking anticyclone. *J. Atmos. Sci. 41*, 3518–3526.

Kalnay, E., Balgovind, R., Chao, W., Edelmann, D., Pfaendtner, J., Takacs, L. and Takano, K. 1983. Documentation of the GLAS fourth order general circulation model. Vol. I *NASA Tech. Memo 86064*, Goddard Space Flight Center, Greenbelt, MD.

Kalnay-Rivas, E., Bayliss, A. and Storch, J. 1977. The 4th order GISS model of the global atmosphere. *Beitr. Phys. Atmos. 50*, 299–311.

Lau, N.-C. and Holopainen, E. O. 1984. Transient eddy forcing of the time-mean flow as identified by geopotential tendencies. *J. Atmos. Sci. 41*, 313–328.

Lejenäs, H. and Økland, H. 1983. Characteristics of northern hemisphere blocking as determined from a long series of observational data. *Tellus 35A*, 350–362.

Mullen, S. L. 1987. Transient eddy forcing of blocking flow. *J. Atmos. Sci. 44*, 3–22.

Pauley, P. M. and Smith, P. J. 1988. Direct and indirect effects of latent heat release on a synoptic-scale wave system. *Mon. Wea. Rev. 166*, 1209–1235.

Rex, D. F. 1950. Blocking action in the middle troposphere and its effect upon regional climate. II. The climatology of blocking action. *Tellus 2*, 275–301.

Shutts, G. J. 1983. The propagation of eddies in diffluent jet streams: Eddy vorticity forcing of blocking flow fields. *Quart. J. Roy. Meteor. Soc. 109*, 737–761.

Smith, P. J. and Tsou, C.-H. 1988. Static stability variations during the development of an intense extratropical cyclone. *Mon. Wea. Rev. 116*, 1245–1250.

Sutera, A. 1986. Probability density distribution of large-scale atmospheric flow. *Adv. Geophys. 29*, 227–249.

Thompson, P. D. 1957. A heuristic theory of large-scale turbulence and long-period velocity variations in barotropic flow. *Tellus 9*, 69–91.

Tsou, C.-H., Smith, P. J. and Pauley, P. M. 1987. A comparison of adiabatic and diabatic forcing in an intense extratropical cyclone system. *Mon. Wea. Rev. 115*, 763–786.

Tung, K. K. and Rosenthal, A. J. 1985. Theories of multiple equilibria—A critical reexamination. Part I: Barotropic models. *J. Atmos. Sci. 42*, 2804–2819.

White, W. B. and Clark, N. E. 1975. On the development of blocking ridge activity over the central North Pacific. *J. Atmos. Sci. 32*, 489–502.